

Thermal noise of beam splitters in laser gravitational wave detectors

Johannes Dickmann,^{1,*} Stefanie Kroker,^{1,2} Yuri Levin,^{3,4,5} Ronny Nawrodt,⁶ and Sergey Vyatchanin^{7,8}

¹*Physikalisch-Technische Bundesanstalt, Bundesallee 100, 38116 Braunschweig, Germany*

²*Technische Universität Braunschweig, LENA Laboratory for Emerging Nanometrology, Pockelsstraße 14, 38106 Braunschweig, Germany*

³*Department of Physics, Columbia University, 704 Pupin Hall, 538 West 120th st, New York, NY 10027, USA*

⁴*Center for Computational Astrophysics, Flatiron Institute, 162 5th Ave, New York, NY 10010, USA*

⁵*School of Physics and Astronomy, Monash University, Clayton, VIC 3800, Australia*

⁶*Physikalisches Institut, Universität Stuttgart, Pfaffenwaldring 57, 70550 Stuttgart, Germany*

⁷*Faculty of Physics, M.V. Lomonosov Moscow State University, Moscow 119991, Russia*

⁸*Quantum Technology Centre, M.V. Lomonosov Moscow State University, Moscow, Russia*

(Dated: January 31, 2022)

We present the calculation of thermal noise in interferometric gravitational-wave detectors due to the thermal fluctuations of the beam splitter (BS). This work makes use of a recently developed method of the analysis of thermal noise in mirrors from first principles, based on the fluctuation dissipation theorem. The evaluation of BS thermal noise is carried out for the two different gravitational wave observatories, GEO600 and the Advanced Laser Interferometer Gravitational Wave Observatory (aLIGO). The analysis evaluates thermal noise from both the substrate and the optical reflective and antireflective stacks located on the BS surface. We demonstrate that the fluctuations of both reflecting and anti-reflecting surfaces significantly contribute to the total thermal noise of the BS. The oscillating intensity pattern couples small-scale distortions of the surface to the overall phase readout, and therefore increases the overall thermal noise. In the case of aLIGO, the BS contribution is with 0.3% negligibly small. At a frequency of 500 Hz, the BS causes about 10% of GEO600's sensitivity limit. BS noise impairs the feasible sensitivity of the GEO-HF design proposal by about 50%.

PACS numbers: 42.79.-e, 04.80.Cc, 05.40.Ca

I. INTRODUCTION

The first direct detections of gravitational waves by the advanced LIGO detectors [1–4] have opened the era of gravitational wave astronomy. These fascinating detection results are a consequence of technology breakthroughs allowing us to measure tiny displacements of $\sim 10^{-18}$ m of macroscopic test masses [5–10]. It is the thermal noise of the test masses that sets a severe limitation for the detector sensitivity in their most sensitive frequency band from 50 Hz to 2000 Hz [11–14]. In current detectors, a major source for thermal noise is Brownian structural noise [15] in mirror coatings. The thermally induced random stresses in the coatings and the substrates of the test masses produce random deformations of their surfaces, which are detected as thermal noise at the interferometer output.

A gravitational wave induces a variation of the frequency of the main mode in the arm cavity of the interferometer, which is registered as a phase shift of a monochromatic optical wave reflected from the cavity. Concurrently, the thermal noise of the mirror's surface also randomly changes the eigenfrequency of the mode masking the gravitational wave signal. The same considerations hold true for the thermal noise of the beam

splitter (BS) in the interferometer. Usually, the beam splitter is a cylindrical plate made of an optically transparent material. One surface is covered by a reflecting (R) coating and the other by an anti-reflecting (AR) one. The thermal fluctuations of *both* surfaces also change the interferometer's eigenfrequency. In previous works, BS noise was estimated by the approximation of BS as infinitely thin plates [16] and in the simplifications of small light beam radii, compared to the BS size and light at normal incidence [17].

In this paper, we present the accurate computation of BS thermal noise in gravitational wave detectors from first principles, following the approach formulated in [18]. In combination with the fluctuation-dissipation theorem (FDT) [19–21] this approach allows the accurate computation of the thermal noise resulting from thermal fluctuations of both R and AR surfaces of BS with light beams of finite size and oblique incidence. A similar approach has been used in [22, 23] for computing thermal noise in reflective gratings and in [24] for evaluating the influence of an absorbing layer on the resonant frequencies and Q-factors of spherical microresonators.

Here we apply our approach for the calculation of Brownian noise in substrate and coating of the BS for arbitrary polarizations of the light. Our estimates show that the contributions of thermoelastic [12] and thermorefractive [13, 25] noise are subdominant to the Brownian noise computed here for frequencies between 100 and 4000 Hz.

*Electronic address: johannes.dickmann@ptb.de

elastic energy stored in the BS due to the applied ponderomotive light pressures. As the surface perturbations are small, we can apply the presented approximations and calculate the pressures with Maxwell stress tensor of the *unperturbed* field in the region around the surface deformation.

A. Calculations of the effective relative displacement (x_-/L)

For the calculation of the terms in (2.7e) it is convenient to use the eigenamplitudes b_{\pm} (2.6b). The work performed against the pressure is equal to the change of energy in the cavity taken with opposite sign. The light pressure p_i acting on dielectric media's surface may be calculated by means of Maxwell stress tensor σ_{ij} inside and outside the material:

$$\sigma_{ij}^{\epsilon} = \frac{1}{4\pi} \left(\epsilon E_i E_j + H_i H_j - \frac{\epsilon E^2 + H^2}{2} \delta_{ij} \right). \quad (2.8)$$

The pressure in (2.8) is directed along the *outer* normal of the surface. For example, for a reflecting surface of the BS, the stress tensor is equal to the pressure acting along (η)-axis (see Fig. 1). In contrast, the stress tensor calculated for the fields directly *beneath* the reflecting surface (inside the BS) is equal to the pressure acting along the ($-\eta$)-axis (compare Fig. 2).

The total normal pressure is equal to the difference of the pressures inside and outside the BS at the surface:

$$p_i = p_i^{\text{outer}} - p_i^{\text{inside}}. \quad (2.9)$$

The relative energy variations $\Delta\mathcal{E}_{\pm}$ can be calculated as the work of ponderomotive light forces resulting from the total normal pressure:

$$\frac{\Delta\mathcal{E}_{\pm}}{\mathcal{E}_{\pm}} = - \int F_{\pm}(\vec{r}_{\perp}) u(\vec{r}_{\perp}) d\vec{r}_{\perp}, \quad F_{\pm} = \frac{p_{\pm}(\vec{r}_{\perp})}{\mathcal{E}_{\pm}}, \quad (2.10)$$

where $u(\vec{r}_{\perp})$ is a small perturbation of the BS surface in normal direction, depending on the coordinate \vec{r}_{\perp} on the

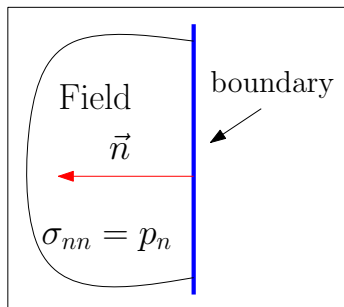


FIG. 2: Maxwell stress tensor σ_{nn} leads to pressure p_n along *outer* normal \vec{n} to the boundary.

BS surfaces. The averaging functions F_{\pm} are defined by the pressures p_{\pm} calculated for the corresponding modes and have to be applied to *both* sides of the BS, as will be shown later. For small perturbations $\Delta\mathcal{E} \ll \mathcal{E}$ the functions F_{\pm} depend only on geometric factors, i.e. surface perturbations, radius of light beam, refractive index and thickness of the BS. They do not depend on the mode amplitudes b_{\pm} , because the energies \mathcal{E}_{\pm} and the pressures p_{\pm} are both proportional to $\sim |b_{\pm}|^2$.

B. Brownian Noise Power Spectral density

Following the FDT [19–21], we have to apply virtual pressures $p(\vec{r}) = F_0 p_{\pm}(\vec{r}) \sin \omega t$, oscillating with an angular frequency ω , to calculate the mean dissipated power $W(\omega)$ in the BS and to finally calculate the Brownian noise power spectral density $S_{BS}(\omega)$:

$$S_{BS}(\omega) = \frac{8k_B T W(\omega)}{\omega^2 F_0^2}, \quad (2.11)$$

where k_B is the Boltzmann constant and T is the absolute temperature. In this paper, we are interested in structural Brownian noise [27]. In the model of structural loss the dissipated power W is defined by the phenomenological loss angle ϕ :

$$W = \mathbb{E} \omega \phi, \quad (2.12)$$

where \mathbb{E} is the mean elastic energy stored in the BS. The pressures on the beam splitter p_{\pm} have striped patterns [18, 28] i.e. which are proportional to $\sim \cos^2 k\xi/\sqrt{2}$ ($k \equiv \omega_0/c$, c is the speed of light). Hence, the applied pressure can be divided into two parts: 1) a smooth (non-striped) pressure P_{sm} and 2) a striped pressure $P_{\text{str}} \sim \cos \sqrt{2}k\xi$. The elastic energies for the problems 1 and 2 can be calculated separately. Indeed, the total energy can be calculated as integral over both sides of the BS:

$$\mathbb{E} = \frac{1}{2} \int (P_{\text{sm}}(\vec{r}_{\perp}) + P_{\text{str}}(\vec{r}_{\perp})) \quad (2.13a)$$

$$\times (u_{\text{sm}}(\vec{r}_{\perp}) + u_{\text{str}}(\vec{r}_{\perp})) d\vec{r}_{\perp} \\ = \mathbb{E}_{\text{sm}} + \mathbb{E}_{\text{str}} + \mathbb{E}_{\times}, \quad (2.13b)$$

$$\mathbb{E}_{\text{sm}} = \frac{1}{2} \int P_{\text{sm}}(\vec{r}_{\perp}) u_{\text{sm}}(\vec{r}_{\perp}) d\vec{r}_{\perp}, \quad (2.13c)$$

$$\mathbb{E}_{\text{str}} = \frac{1}{2} \int P_{\text{str}}(\vec{r}_{\perp}) u_{\text{str}}(\vec{r}_{\perp}) d\vec{r}_{\perp} \quad (2.13d)$$

$$\mathbb{E}_{\times} = \frac{1}{2} \int [P_{\text{sm}}(\vec{r}_{\perp}) u_{\text{str}}(\vec{r}_{\perp}) + P_{\text{str}}(\vec{r}_{\perp}) u_{\text{sm}}(\vec{r}_{\perp})] d\vec{r}_{\perp}, \quad (2.13e)$$

where $u_{\text{sm}}(\vec{r}_{\perp})$ and $u_{\text{str}}(\vec{r}_{\perp})$ are surface displacements caused by smooth and striped pressures, respectively. Obviously, the cross term of energy \mathbb{E}_{\times} will be negligibly small after integration over the surface, due to the fast oscillating multiplier $\cos \sqrt{2}k\xi$. To our best knowledge, there is no approach to solve problem 1 analytically.

Hence, we solve it numerically using the finite element tool COMSOL Multiphysics [29]. In contrast, problem 2 can be solved analytically using the well-known solution for a half infinite elastic media [28]. This method can be applied, because the pressure contribution with fast spatial oscillation, characterized by the wave vector k_0 , leads only to deformations located close to the surface. In particular, the elasticity divergence $\Theta = u_{xx} + u_{yy} + u_{zz}$ decreases along the z -axis normal to the surface as $\sim e^{-kz}$.

III. CALCULATIONS OF PRESSURES

We assume all light beams in the interferometer to have an amplitude Gaussian distribution over the cross section:

$$f_0(r_\perp) = \frac{e^{-r_\perp^2/2r_0^2}}{\sqrt{\pi r_0^2}}, \quad \int |f_0|^2 d\vec{r}_\perp = 1, \quad (3.1)$$

where $d\vec{r}_\perp \equiv r_\perp dr_\perp d\phi$. For gravitational wave detectors we can assume that the beam radius r_0 is *large*:

$$r_0 \gg \lambda = \frac{2\pi}{k}, \quad (3.2)$$

where λ is the wavelength. Hence, we can consider the wave in the cavity as a plane wave with an amplitude multiplied by the Gaussian factor f_0 omitting terms of higher orders $\sim 1/kr_0$ (see for example [30–32]). For the calculations, we introduce the following relations between the coordinates (x_e, x_n) and (ξ, η) (see Fig. 1):

$$x_e = \frac{\xi - \eta}{\sqrt{2}}, \quad x_n = \frac{\xi + \eta}{\sqrt{2}}, \quad (3.3)$$

$$\xi = \frac{x_e + x_n}{\sqrt{2}}, \quad \eta = \frac{-x_e + x_n}{\sqrt{2}}. \quad (3.4)$$

Inside the BS the light propagates with an angle α with respect to the BS axis (see Fig. 4):

$$\sin \alpha = \frac{1}{n\sqrt{2}}, \quad 2a = h \tan \alpha. \quad (3.5)$$

On the AR surface there are two centers of Gaussian distributions separated by distance $2a$ (see Fig. 4). Inside the BS, the beams propagate along the axes y_e, y_n . These coordinates may be recalculated from the coordinates (ξ, η) :

$$y_e = \xi \sin \alpha + \eta \cos \alpha, \quad (3.6)$$

$$y_n = \xi \sin \alpha - \eta \cos \alpha. \quad (3.7)$$

We calculate the fields and pressures for different polarizations of traveling waves: S-polarization (vector of electric field is normal to the plane of figure) and p-polarization (vector of magnetic field is normal to the plane of figure). As a result, after simple but cumbersome calculations presented in Appendix A, we obtain the averaging functions on both surfaces of the BS and for each polarization orientation. We present these functions in the following 2 subsections.

A. S-polarization summary

For the GEO600 interferometer and s-polarization, we obtain the following equation for the eigenfrequency shift, i.e. effective relative displacement x_-/L . For the reflecting surface R of the BS we retrieve using (2.7e) and (A6f, A21)

$$\frac{x_-}{L} \Big|_{rS} = \int \frac{F_r^s(\vec{r}_\perp)}{L} u_\perp(\vec{r}_\perp) d\vec{r}_\perp, \quad (3.8)$$

$$\frac{F_r^s(\vec{r}_\perp)}{L} \equiv \left(\frac{p^{rS+}}{\mathcal{E}_+} - \frac{p^{rS-}}{\mathcal{E}_-} \right) \quad (3.9)$$

$$= \frac{f_\perp^2}{2L} \left\{ \left[2n - \frac{1}{n} + 1 \right] - \left[1 + \frac{1}{n} + 2\sqrt{2}(n-1) \right] \cos 2k_{bs}\xi \right\}, \quad (3.10)$$

where we use the notations of (3.5) and

$$k_{bs} = \frac{k}{\sqrt{2}}, \quad (3.11)$$

$$f_\perp \equiv \frac{1}{\sqrt{\pi r_0^2}} \exp\left(-\frac{z^2 + 0.5\xi^2}{2r_0^2}\right). \quad (3.12)$$

For the anti-reflecting surfaces AR of the BS we get with (2.7e) and (A13, A27):

$$\frac{x_-}{L} \Big|_{arS} = \int \frac{F_{ar}^s(\vec{r}_\perp)}{L} u_\perp(\vec{r}_\perp) d\vec{r}_\perp, \quad (3.13)$$

$$\frac{F_{ar}^s(\vec{r}_\perp)}{L} \equiv \left(\frac{p^{arS+}}{\mathcal{E}_+} - \frac{p^{arS-}}{\mathcal{E}_-} \right) \quad (3.14)$$

$$= \frac{1}{2L} \left\{ (f_+^2) \left[1 - 2n + \frac{1}{n} \right] + 2\sqrt{2}(n-1)f_- f_+ \cos \kappa(\xi_+ + \xi_-) - f_+^2 \left(1 - \frac{1}{n} \right) \cos 2\kappa\xi_+ \right\}. \quad (3.15)$$

Here, we use the following notations (3.5, 3.11, 3.12) and definitions:

$$f_\pm = \sqrt{\frac{1}{\pi r_0^2}} \exp\left(-\frac{z^2 + 0.5(\xi \mp a)^2}{2r_0^2}\right), \quad (3.16)$$

$$\xi_\pm \equiv \xi \mp a. \quad (3.17)$$

B. P-polarization summary

For the GEO600 interferometer and p-polarization, we obtain the following equations for the eigenfrequency shift, i.e. effective x_-/L . For the surfaces R we get using (2.7e) and (A35, A51)

$$\frac{x_-}{L} \Big|_{rP} = \int \frac{F_r^p(\vec{r}_\perp)}{L} u_\perp(\vec{r}_\perp) d\vec{r}_\perp, \quad (3.18)$$

$$\frac{F_r^p(\vec{r}_\perp)}{L} \equiv \left(\frac{p^{rP+}}{\mathcal{E}_+} - \frac{p^{rP-}}{\mathcal{E}_-} \right) \quad (3.19)$$

$$= \frac{f_\perp^2}{2L} \left\{ \left[2n - \frac{1}{n} + 1 \right] + \left[1 + \frac{1}{n} + 2\sqrt{2}(n-1) \right] \cos \sqrt{2}k\xi \right\}. \quad (3.20)$$

For the surface AR we get using (2.7e) and (A43, A57)

$$\frac{x_-}{L} \Big|_{arP} = \int \frac{F_{ar}^p(\vec{r}_\perp)}{L} u_\perp(\vec{r}_\perp) d\vec{r}_\perp, \quad (3.21)$$

$$\frac{F_{ar}^p(\vec{r}_\perp)}{L} \equiv \left(\frac{p^{arP+}}{\mathcal{E}_+} - \frac{p^{arP-}}{\mathcal{E}_-} \right) \quad (3.22)$$

$$= \frac{1}{2L} \left\{ (f_+^2) \left[1 - 2n + \frac{1}{n} \right] - 2\sqrt{2}(n-1)f_-f_+ \cos \kappa(\xi_+ + \xi_-) + (f_+^2) \left(1 - \frac{1}{n} \right) \cos 2k_{bs}\xi_+ \right\}. \quad (3.23)$$

We see that the "smooth" parts of the pressure acting on R and AR surfaces are the same both for p- and s-polarizations (compare (3.10) with (3.20) and (3.15) with (3.23)). However, the "striped" contributions have opposite signs for s- and p-polarization while being equal in their absolute value. Hence, for non-polarized light and for the case of equal s- and p-polarized field amplitudes, the "striped" term vanishes.

C. Generalization for the aLIGO interferometers

The results in subsections III A and III B are obtained for the GEO600 configuration *without* input mirrors (IM), shown by dashed rectangles in Fig. 1. For the calculation of the mode energies \mathcal{E}_\pm , we use the fact, that the amplitudes of the fields on BS are nearly the same as in the arms, and in addition we utilize the approximation (2.2). For advanced LIGO, we have to recalculate the energies \mathcal{E}_\pm by taking into account, that the mean amplitudes in the arms are by a factor of approximately $2/\sqrt{T_{\text{IM}}}$ larger than on the BS. Here T_{IM} represents the power transmittance of the IM. Hence, we can generalize, for example, formula (3.10) for s-polarization on the R surface by the transformation:

$$F_r^s|_{\text{GEO}} = F_r^s|_{\text{aLIGO}} \times \frac{T_{\text{IM}}}{4}. \quad (3.24)$$

Obviously, the other formulas (3.15, 3.20, 3.23) can be generalized for advanced LIGO using the same transformation (3.24).

IV. CALCULATION OF THE ELASTIC ENERGY

To calculate the spectral density of the Brownian BS noise in terms of relative displacements x_-/L for s-

polarization, we have to apply virtual pressures p_{rs} to the R surface of the BS using (3.10) and p_{ars} to the AR surface using (3.15):

$$p_{rs} = F_0 F_r^s(\vec{r}) \sin \omega t, \quad p_{ars} = F_0 F_{ar}^s(\vec{r}) \sin \omega t, \quad (4.1)$$

where F_0 is a constant, see (2.11). For the p-polarization we should use (3.20, 3.23). Then we calculate the mean elastic energy \mathbb{E} stored in the BS and substitute this result into (2.11) by taking (2.12) into account. Since the elastic problem cannot be solved analytically, we perform the computations numerically using COMSOL [29]. We use the parameters for the BS of GEO600 and advanced LIGO listed in Table I. For the following considerations, we account only for the smooth contributions of the pressures (4.1), which are equal for both polarizations (see (3.10, 3.15, 3.20, 3.23)). For the solution of the elastic problem, we have to fulfill two conditions: a) the sum of all external forces and b) the total torque of all external forces should be equal to zero. However, the pressures integrated over the R and the AR surfaces are not equal to zero, i.e. the total force acting on the BS is not equal to zero. Hence, in analogy to inertial forces we have to apply an additional volume force f , which is *homogeneously distributed* over the BS such that the total force is equal to zero [33]:

$$f = -\frac{1}{\pi R^2 h} \int [p_r(\vec{r}_\perp) + p_{ar}(\vec{r}_\perp)] dS = \quad (4.2)$$

$$= -\frac{\sqrt{2}F_0}{\pi R^2 h} \times (1 - \epsilon_F), \quad (4.3)$$

where the integration is performed over the area of the BS, having radius R and height h . In approximation $R \rightarrow \infty$, the coefficient ϵ_F is zero. For the parameters of

TABLE I: Parameters of BS for GEO600 and aLIGO.

Parameters	aLIGO	GEO600
Radius R of BS, m	0.1875	0.13
Height h of BS, m	0.064	0.08
Refractive index n_{SiO_2}	1.45	1.45
$a = \frac{h}{\sqrt{2n^2-1}}$	0.036	0.045
Radius $w_0 = \sqrt{2}r_0$ of light beam on BS, m ^a	0.06	0.0088
Young's modulus E_{SiO_2} , GPa	73.1	73.1
Poisson's ratio ν_{SiO_2}	0.17	0.17
Density ρ_{SiO_2} , kg/m ³	2203	2203
Loss angle ϕ_{SiO_2}	10^{-8}	10^{-8}
Power transmittance of input mirrors in arms of aLIGO	5×10^{-3}	—

^a r_0 is the beam radius for the *intensity* distribution, which is proportional to $\sim \exp[-r^2/r_0^2]$, whereas w_0 is the radius for the *amplitude* distribution, which is proportional to $\sim \exp[-r^2/w_0^2]$. So $w_0 = \sqrt{2}r_0$.

advanced LIGO and GEO600 in Table I, the numerical computations yield:

$$\epsilon_F^{\text{LIGO}} \simeq -0.000142, \quad (4.4)$$

$$\epsilon_F^{\text{GEO}} \simeq 3.3 \times 10^{-16}. \quad (4.5)$$

The total torque of the external forces is not zero, because the centre of p_{ar} is shifted from the symmetrical cylinder axis by distance a . Hence, we have to introduce an additional volume force $f_{\text{add}} \sim y/R$ in order to eliminate effective torques:

$$f_{\text{add}} = (1 - \epsilon_T) \frac{\sqrt{2} F_0}{\pi R^2 h} \left(1 - 2n + \frac{1}{n}\right) \times \frac{2ay}{R^2}, \quad (4.6)$$

where the small coefficient ϵ_T results from the finite dimension of the BS. In the approximation $R \rightarrow \infty$, we retrieve $\epsilon_T \rightarrow 0$. For the parameters in Table I, numerical computations lead to:

$$\epsilon_T^{\text{LIGO}} \simeq 0.00576962, \quad (4.7)$$

$$\epsilon_T^{\text{GEO}} \simeq 1.19 \times 10^{-13}. \quad (4.8)$$

1. Substrate thermal Brownian noise of the BS

In order to calculate Brownian noise from thermal fluctuation in the BS substrate, we calculate the mean elastic energy stored in the BS. Using COMSOL, we performed numerical calculations of the mean elastic energy for parameters in Table I:

$$\mathbb{E}_{\text{aLIGO}} = 3.98 \times 10^{-10} \text{ J} \times \frac{F_0^2}{N^2}, \quad (4.9)$$

$$\mathbb{E}_{\text{GEO}} = 1.97 \times 10^{-9} \text{ J} \times \frac{F_0^2}{N^2}. \quad (4.10)$$

Using (2.11), we compute the power spectral density S_{BS} of the BS Brownian noise, recalculated to the differential coordinate x_- :

$$\left. \frac{\sqrt{S_{\text{BS}}(\omega)}}{L} \right|_{\text{LIGO}} \simeq 4.5 \times 10^{-27} \frac{1}{\sqrt{\text{Hz}}}, \quad (4.11)$$

$$\left. \frac{\sqrt{S_{\text{BS}}(\omega)}}{L} \right|_{\text{GEO}} \simeq 2.7 \times 10^{-23} \frac{1}{\sqrt{\text{Hz}}}, \quad (4.12)$$

at the angular frequency $\omega = 2\pi \times 100 \text{ s}^{-1}$ for advanced LIGO and GEO600, respectively. For advanced LIGO we have taken the transformation (3.24) into account. The current sensitivity of advanced LIGO [8] is about $\sqrt{S_x}/L \simeq 5 \times 10^{-23} \text{ 1}/\sqrt{\text{Hz}}$, for the future cryogenic LIGO Voyager [34] the planned sensitivity is about $\sqrt{S_x}/L \simeq 8 \times 10^{-25} \text{ 1}/\sqrt{\text{Hz}}$. Since the substrate BS noise is substantially smaller than this sensitivity, LIGO Voyager will not be limited by it. The current sensitivity of GEO600 [10] is about $\sqrt{S_x}/L \simeq 3 \times 10^{-22} \text{ 1}/\sqrt{\text{Hz}}$. It is about 10 times larger than BS noise evaluated here.

2. Coating thermal Brownian noise of the BS

The Brownian noise of the R and AR coatings has to be calculated separately, because the loss angle of the alternating layers of Ta_2O_5 and SiO_2 are much larger than the loss of the substrate. These coatings are required to provide the optical function of the reflective and anti-reflective BS surfaces. For advanced LIGO, the parameters of the BS coatings are listed in Table II. The parameters of the GEO600 coatings are not published. Therefore, we assume the optical coating design to be the same as for LIGO (see Table II). We calculate the energy stored in the coatings with the assumption that the coatings are thin compared to the BS thickness. Thus, the strains in the layers are approximately the same as on the upper side of the substrate. We use the following expression for the volume density w of elastic energy in the layer [27, 28]:

$$w_n = \frac{1}{2} \frac{(1 + \nu)(1 - 2\nu)\sigma_{zz}^2}{Y(1 - \nu)} + \frac{Y(u_{xx} + u_{yy})^2}{4(1 - \nu)} + \frac{Y(u_{xx} - u_{yy})^2}{4(1 + \nu)} + \frac{Y}{1 + \nu} \times u_{xy}^2. \quad (4.13)$$

Here σ_{zz} is the normal component of the stress tensor, Y and ν are Young's modulus and Poisson's ratio of the layers (made of Ta_2O_5 or SiO_2), whereas u_{ij} are the tangent components of the strain tensors, which are the same as for the substrate's surface. The total energy stored in the SiO_2 and Ta_2O_5 layers of the R and the AR coatings can be calculated as:

$$\mathbb{E}_{\text{coat}} = h_r \text{SiO}_2 \int w_n|_{r \text{SiO}_2} dS_r \quad (4.14)$$

$$+ h_r \text{Ta}_2\text{O}_5 \int w_n|_{r \text{Ta}_2\text{O}_5} dS_r \quad (4.15)$$

$$+ h_{ar \text{SiO}_2} \int w_n|_{ar \text{SiO}_2} dS_r \quad (4.16)$$

$$+ h_{ar \text{Ta}_2\text{O}_5} \int w_n|_{ar \text{Ta}_2\text{O}_5} dS_r, \quad (4.17)$$

where the integration is carried out over the R and AR surfaces. Performing a numeric integration using u_{ij} , ob-

TABLE II: Parameters of the reflecting and anti-reflecting coatings of the BS for advanced LIGO [35, 36].

Parameters	SiO_2	Ta_2O_5
Refractive index	1.45	2.1
Young modulus, GPa	73.1	140
Poisson ratio	0.17	0.23
Loss angle	1×10^{-4}	4×10^{-4}
R coating total thickness h_r , nm	523	320
AR coating total thickness h_{ar} , nm	517	359

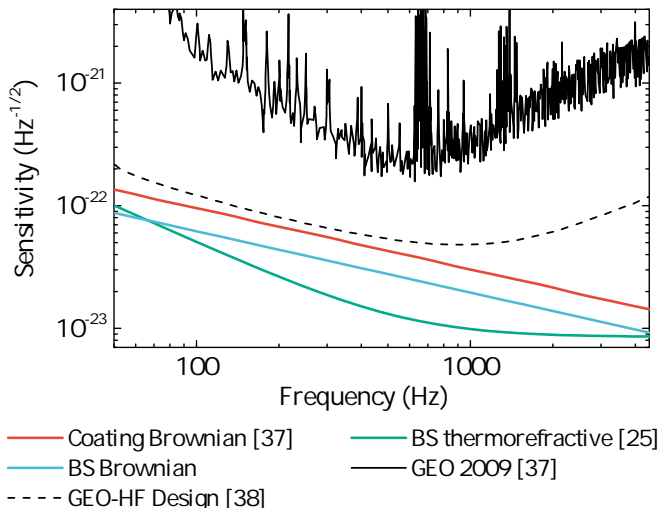


FIG. 3: Noise \sqrt{S}/L of GEO600 in $1/\sqrt{\text{Hz}}$ versus mechanical readout frequency f for the following thermal noise contributions: The mirror coating Brownian [37], the BS thermorefractive [25] and the BS Brownian noise computed in this work. Additionally, the measured sensitivity of 2009 [37] and the design sensitivity of GEO-HF [38] are shown.

tained for the substrate and the parameters listed in Table II, we obtain at $\omega = 2\pi 100 \text{ s}^{-1}$:

$$\left. \frac{\sqrt{S_{\text{BS}}(\omega)}}{L} \right|_{\text{GEO}} \simeq 6.2 \times 10^{-23} \frac{1}{\sqrt{\text{Hz}}}, \quad (4.18)$$

$$\left. \frac{\sqrt{S_{\text{BS}}(\omega)}}{L} \right|_{\text{LIGO}} \simeq 0.98 \times 10^{-26} \frac{1}{\sqrt{\text{Hz}}} \quad (4.19)$$

Fig. 3 shows the BS Brownian noise in comparison to the other severe limitations of the GEO600 sensitivity, namely the mirror coating Brownian and the beamsplitter thermorefractive noise. Over the whole detection bandwidth of GEO600, the BS Brownian noise is about 35% lower than the mirror coating Brownian noise. For frequencies larger than 100 Hz, the BS Brownian noise is more dominant than the BS thermorefractive noise. At the most sensitive frequency of GEO at 500 Hz, the BS noise (4.18) accounts for approximately 10% of the current sensitivity. Fig. 3 shows also the sensitivity curve of the proposed GEO-HF upgrade [38]. This curve so far does not take the BS Brownian noise into account. As illustrated in Fig. 3, the BS Brownian noise impairs the feasible sensitivity of the GEO-HF by about 50% for the frequency range between 50 and 1000 Hz.

V. CONCLUSION

In this contribution we applied the direct method of thermal noise calculations from first principles formulated in [18], to the computation of Brownian thermal

noise of beam splitters in gravitational wave interferometers. We have demonstrated how the light pressure on both reflective and anti-reflective surfaces contributes to the total thermal noise of the BS. To this end, we took finite sized BS substrates and the coating contributions into account. An important new ingredient on our calculations is taking into account the striped pattern of the form-factor that represents the sensitivity of the interferometers readout to the BS surface displacement. The pattern is due to the standing waves inside each of the arms¹ The striped contribution of the pressure turns out to be negligibly small for the substrate Brownian noise. But it provides an increase of the total spectral density of coating Brownian noise by about 50% (see Sec. IVB of [28]).

The results show, that the BS noise is negligibly small for advanced LIGO. However, for GEO600, it accounts for about 10% of the current noise budget in the most sensitive frequency band. Furthermore, BS noise impairs the feasible sensitivity of the proposed GEO-HF design by about 50%. This is because the additional Fabry-Perot arm cavities in LIGO lead to smaller light powers at the BS, compared to the power circulating in the arms. Hence, the BS noise in comparison to the test mass noise is suppressed. Whereas in GEO600, the contribution of BS noise is much larger, because the light power at the BS is the same as at the test masses. Overall, the Brownian BS noise is not a critical issue for the current sensitivity of gravitational wave detectors. However, the presented approach is based on a first-principle method with the Hamiltonian as starting point. It is thus useful for noise computations in other interferometer topologies, for example Sagnac interferometers or other complex optical devices.

Acknowledgments

We are grateful to Garilynn Billingsley for providing us with the information about the thickness of the coating layers on the aLIGO beamsplitters. S.K. acknowledges partial support from EURAMET within project 17FUN05 PhotOQuant. S.V. acknowledges partial support from the Russian Science Foundation (Grant No. 17-12-01095) and from the TAPIR GIFT MSU Support of the California Institute of Technology. This document has LIGO number P1800211-v1.

¹ We note that similar standing-wave patterns are important in computations of thermoelastic [12] and thermorefractive [13, 25] noise of the BS.

Appendix A: Calculation details for fields and pressures

In this appendix we present in detail the derivations of the functions f_{\pm} , describing the pressure distributions on both BS sides for two (“plus” and “minus”) modes defined by (2.6). We consider separately s- and p-polarization of the circulating light waves.

1. S-polarization. B_+ mode

For the pressure, we have to calculate the fields on the R and on AR surface inside and outside the BS. We begin with the B_+ mode and s-polarization, see Fig. 4, denoted by B_+ amplitude of the magnetic field inside the east arm, whereas the wave in north arm is absent. The z -axis is directed *out of* plane. The electric field components are denoted as E , the magnetic ones by H and subscripts denote projections.

Surface 1R. For the complex amplitudes of electric and magnetic fields we obtain (see Fig. 4 and definition (3.11)):

$$E_z = \frac{B_+}{\sqrt{2}} (e^{ik_x e} - e^{-ik_x e})_{\eta=0} \quad (\text{A1a})$$

$$= i\sqrt{2} B_+ \sin(k_{bs}\xi),$$

$$H_n = -\frac{B_+}{\sqrt{2}} (e^{ik_x e} + e^{-ik_x e})_{\eta=0} \quad (\text{A1b})$$

$$= -\sqrt{2} B_+ \cos(k_{bs}\xi),$$

$$H_{\xi} = H_{\eta} = \frac{H_n}{\sqrt{2}} = -B_+ \cos(k_{bs}\xi). \quad (\text{A1c})$$

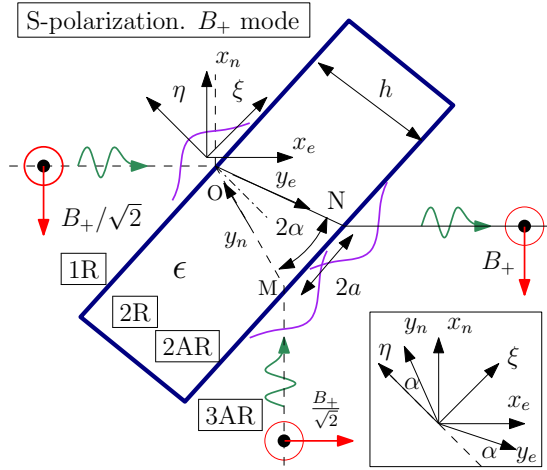


FIG. 4: B_+ mode, s-polarization, i.e. electrical field is normal to the plane of the figure, a fat dot means that it is directed *out of* the plane, a cross *into* the plane, respectively. The red arrows indicate the direction of the magnetic field.

Using definition (2.8) we calculate the Maxwell stress tensor on surface 1R:

$$\sigma_{\eta\eta} = -\frac{|B_+|^2}{2\pi} \sin^2(k_{bs}\xi). \quad (\text{A2})$$

Component $\sigma_{\eta\eta}$ corresponds to the pressure acting *along* axis η , hence $p_{\eta} = \sigma_{\eta\eta}$. The spatial distribution of the pressure p_{η} should be restored in (A2), by projecting (3.1) on the reflecting surface R:

$$p_{\eta}^{1rS+} = -\frac{|B_+|^2}{4\pi} (1 - \cos 2k_{bs}\xi) f_{\perp}^2, \quad (\text{A3})$$

see definition (3.12). The pressure consists of a smooth contribution and a fast oscillating one $\sim \cos 2k_{bs}\xi$.

Surface 2R (s-polarization, B_+ mode). The relationship between the electric and magnetic fields inside the material (marked by superscript ϵ) and the light intensity is:

$$|H^{\epsilon}| = \sqrt{\epsilon} |E^{\epsilon}|, \quad I_{\epsilon} = c \frac{\sqrt{\epsilon} |E^{\epsilon}|^2}{4\pi}, \quad n \equiv \sqrt{\epsilon}. \quad (\text{A4})$$

The intensity inside and outside the BS of AR surface has to be conserved. Thus, for the amplitudes of the wave propagating along y_n - and y_e - axes and inside the BS:

$$E_z = \frac{B_+}{\sqrt{n}\sqrt{2}} (e^{ink_y n} - e^{-ink_y n}) \quad (\text{A5a})$$

$$+ \frac{B_+}{\sqrt{n}} (e^{ink_y e} - e^{-ink_y e}),$$

$$E_z|_{\eta=0} = \frac{i\sqrt{2}(\sqrt{2}+1)B_+}{\sqrt{n}} \sin(k_{\alpha}\xi), \quad (\text{A5b})$$

$$k_{\alpha} = nk \sin \alpha = k_{bs}, \quad (\text{A5c})$$

$$\sin \alpha = \frac{1}{\sqrt{2}n}, \quad \cos \alpha = \sqrt{1 - \frac{1}{2n^2}}, \quad (\text{A5d})$$

$$H_{\eta} = -\frac{B_+\sqrt{n} \sin \alpha}{\sqrt{2}} (e^{ink_y n} + e^{-ink_y n}) \quad (\text{A5e})$$

$$- B_+\sqrt{n} \sin \alpha (e^{ink_y e} + e^{-ink_y e}),$$

$$H_{\eta}|_{\eta=0} = -\sqrt{2n} \sin \alpha (\sqrt{2}+1) B_+ \cos k_{bs}\xi, \quad (\text{A5f})$$

$$H_{\xi} = \frac{B_+\sqrt{n} \cos \alpha}{\sqrt{2}} (e^{ink_y n} + e^{-ink_y n}) \quad (\text{A5g})$$

$$- B_+\sqrt{n} \cos \alpha (e^{ink_y e} + e^{-ink_y e})$$

$$H_{\xi}|_{\eta=0} = \sqrt{2n} \cos \alpha (1 - \sqrt{2}) B_+ \cos k_{bs}\xi. \quad (\text{A5h})$$

We calculate the Maxwell stress tensor at the surface 2R, using definition (2.8) again:

$$\sigma_{\eta\eta} = -\frac{n|B_+|^2}{4\pi} \left\{ 3(1 + \cos 2\alpha) - [3 - 3\cos 2\alpha + 4\sqrt{2}] \cos 2k_{bs}\xi \right\}. \quad (\text{A6a})$$

The spatial distribution of the pressure p_{η} should be restored in (A6a), by projecting (3.1) on the reflecting surface of the BS:

$$p_{\eta}^{2rS+} = \frac{n|B_+|^2}{4\pi} \left\{ 3(1 + \cos 2\alpha) \right\} \quad (\text{A6b})$$

$$- \left[3 - 3 \cos 2\alpha + 4\sqrt{2} \right] \cos 2k_{bs}\xi \} f_{\perp}^2.$$

The total pressure applied to the surface R of BS (s-polarization, B_+ mode) is equal to the *sum* of (A3) and (A6b):

$$p_{\eta}^{rS+} = p_{\eta}^{1rS+} + p_{\eta}^{2rS+} \quad (\text{A6c})$$

$$= \frac{|B_+|^2 f_{\perp}^2}{4\pi} \left\{ 3n(1 + \cos 2\alpha) - 1 \right. \\ \left. + \left(1 - n \left[3 - 3 \cos 2\alpha + 4\sqrt{2} \right] \right) \cos 2k_{bs}\xi \right\}, \quad (\text{A6d})$$

We calculate \mathcal{E}_+ of this mode using the assumption (2.2) and the expression for the function f_0 (3.1):

$$\mathcal{E}_+ = \frac{|B_+|^2}{\pi} \left(L + \frac{\ell_s + \ell_w}{2} \right) \simeq \frac{|B_+|^2 L}{\pi}. \quad (\text{A6e})$$

Using definitions (2.10), we get:

$$\frac{p_{\eta}^{rS+}}{\mathcal{E}_+} = \frac{f_{\perp}^2}{4L} \left\{ 3n(1 + \cos 2\alpha) - 1 \right. \\ \left. + \left(1 - n \left[3 - 3 \cos 2\alpha + 4\sqrt{2} \right] \right) \cos 2k_{bs}\xi \right\} \quad (\text{A6f})$$

Surface 3AR (s-polarization, B_+ mode). The distributions of fields from south and east arm are shifted by $\pm a$ from the center as shown in Fig. 4, $2a = h \tan \alpha$. Using definitions (3.16, 3.17) we obtain:

$$E_z = \frac{B_+}{\sqrt{2}} (e^{ikx_n} - e^{-ikx_n}) f_- \\ + B_+ (e^{ikx_e} - e^{-ikx_e}) f_+, \quad (\text{A7a})$$

$$E_z|_{\eta=-h} = i\sqrt{2}B_+ \left(\sin \left(\frac{k\xi_-}{\sqrt{2}} \right) f_- \right. \\ \left. + \sin \left(\frac{k\xi_+}{\sqrt{2}} \right) \sqrt{2}f_+ \right), \quad (\text{A7b})$$

$$H_{\xi} = \frac{B_+}{\sqrt{2}} (e^{ikx_n} + e^{-ikx_n}) \frac{f_-}{\sqrt{2}} \\ - B_+ (e^{ikx_e} + e^{-ikx_e}) \frac{f_+}{\sqrt{2}}, \quad (\text{A7c})$$

$$H_{\xi}|_{\eta=-h} = B_+ \left(\cos \left(\frac{k\xi_-}{\sqrt{2}} \right) f_- \right. \\ \left. - \cos \left(\frac{k\xi_+}{\sqrt{2}} \right) \sqrt{2}f_+ \right), \quad (\text{A7d})$$

$$- \cos \left(\frac{k\xi_+}{\sqrt{2}} \right) \sqrt{2}f_+, \quad (\text{A7e})$$

$$H_{\eta} = -\frac{B_+}{\sqrt{2}} (e^{ikx_n} + e^{-ikx_n}) \frac{f_-}{\sqrt{2}} \\ - B_+ (e^{ikx_e} + e^{-ikx_e}) \frac{f_+}{\sqrt{2}}, \quad (\text{A7f})$$

$$H_{\eta}|_{\eta=-h} = -B_+ \cos \left(\frac{k\xi_-}{\sqrt{2}} \right) f_- \\ + B_+ \cos \left(\frac{k\xi_+}{\sqrt{2}} \right) \sqrt{2}f_+. \quad (\text{A7g})$$

We calculate Maxwell stress tensor on 3AR surface of BS using definition (2.8) again:

$$\sigma_{\eta\eta} = \frac{|B_+|^2}{4\pi} \left\{ -f_-^2 - 2f_+^2 4\sqrt{2} f_- f_+ \cos k_{bs}(\xi_+ + \xi_-) \right. \\ \left. + f_-^2 \cos 2\kappa\xi_- + 2f_+^2 \cos 2\kappa\xi_+ \right\}. \quad (\text{A8})$$

The pressure along the η -axis reads:

$$p_{\eta}^{3arS} = -\sigma_{\eta\eta}. \quad (\text{A9})$$

Surface 2AR of the BS (S-polarization, B_+ mode):

$$E_z = \frac{B_+}{\sqrt{2}n} (e^{inky_n} - e^{-inkx_n}) f_- \\ + \frac{B_+}{\sqrt{n}} (e^{inky_e} - e^{-inky_e}) f_+, \quad (\text{A10a})$$

$$E_z|_{\eta=-h} = \frac{i\sqrt{2}B_+}{\sqrt{n}} \quad (\text{A10b})$$

$$\times \left[f_- \sin k_{bs}\xi_- + \sqrt{2}f_+ \sin k_{bs}\xi_+ \right],$$

$$H_{\xi} = \frac{B_+\sqrt{n}}{\sqrt{2}} (e^{inky_n} + e^{-inky_n}) f_- \cos \alpha \\ - B_+\sqrt{n} (e^{inky_e} + e^{-inky_e}) f_+ \cos \alpha, \quad (\text{A10c})$$

$$H_{\xi}|_{\eta=-h} = \sqrt{2}\sqrt{n}B_+ \cos \alpha \\ \times \left(f_- \cos \kappa\xi_- - \sqrt{2}f_+ \cos \kappa\xi_+ \right), \quad (\text{A10d})$$

$$H_{\eta} = -\frac{B_+\sqrt{n}}{\sqrt{2}} (e^{inky_n} + e^{-inky_n}) f_- \sin \alpha \\ + B_+\sqrt{n} (e^{inky_e} + e^{-inky_e}) f_+ \sin \alpha, \quad (\text{A10e})$$

$$H_{\eta}|_{\eta=-h} = -\sqrt{2}\sqrt{n}B_+ \sin \alpha \\ \times \left(f_- \cos \kappa\xi_- + \sqrt{2}f_+ \cos \kappa\xi_+ \right). \quad (\text{A10f})$$

Maxwell stress tensor *at* the surface 2AR of the BS:

$$\sigma_{\eta\eta} = \frac{n|B_+|^2}{2\pi} \left\{ -(f_-^2 + 2f_+^2) \cos^2 \alpha \right. \\ \left. + (f_-^2 \cos 2\kappa\xi_- + 2f_+^2 \cos 2k_{bs}\xi_+) \sin^2 \alpha \right. \\ \left. + 2\sqrt{2}f_+f_- \cos k_{bs}(\xi_+ + \xi_-) \right\}. \quad (\text{A11})$$

Pressure along the η -axis: $p_{\eta}^{2arS+} = \sigma_{\eta\eta}$. So, the total pressure along the η -axis on surface 2AR of the BS (s-polarization, B_+ mode) is equal to:

$$p_{\eta}^{arS+} = p_{\eta}^{2arS+} + p_{\eta}^{3arS+}, \quad (\text{A12})$$

$$\frac{p_{\eta}^{2arS+} + p_{\eta}^{3arS+}}{\mathcal{E}_+} \quad (\text{A13})$$

$$= \frac{1}{4L} \left\{ (f_-^2 + 2f_+^2) \left[1 + \frac{1}{n} - 2n \right] \right. \\ \left. + 4\sqrt{2}(n-1)f_-f_+ \cos k_{bs}(\xi_+ + \xi_-) \right. \\ \left. + (f_-^2 \cos 2k_{bs}\xi_- + 2f_+^2 \cos 2k_{bs}\xi_+) \left(-1 + \frac{1}{n} \right) \right\}.$$

2. S-polarization. B_- mode

The geometry is shown in Fig. 5, the z -axis is directed *out of* the plane of figure. B_- indicates the amplitude of the magnetic field in the north arm, the wave is absent in the east arm.

Surface 1R of BS (s-polarization, B_- mode):

$$E_z = \frac{-B_-}{\sqrt{2}} (e^{ikx_e} - e^{-ikx_e}) + B_- (e^{ikx_n} - e^{-ikx_n}), \quad (\text{A14a})$$

$$E_z|_{\eta=0} = i\sqrt{2}B_- (\sqrt{2} - 1) \sin k_{bs}\xi, \quad (\text{A14b})$$

$$H_\eta|_{\eta=0} = (1 - \sqrt{2})B_- \cos k_{bs}\xi, \quad (\text{A14c})$$

$$H_\xi|_{\eta=0} = (1 + \sqrt{2})B_- \cos k_{bs}\xi, \quad (\text{A14d})$$

Maxwell stress tensor on surface 1R:

$$\sigma_{\eta\eta} = -\frac{|B_-|^2}{4\pi} \left(3 + [4\sqrt{2} - 3] \cos 2k_{bs}\xi \right). \quad (\text{A15})$$

The component $\sigma_{\eta\eta}$ corresponds to the pressure acting *along* the η -axis, hence $p_\eta = -\sigma_{\eta\eta}$. A negative sign in (A15) means, that the field *pushes* the BS. The spatial distribution of the pressure p_η has to be restored in (A15), by projecting (3.1) on the reflecting surface of BS:

$$p_\eta^{1rS-} = -\frac{|B_-|^2}{4\pi} \left(3 + [4\sqrt{2} - 3] \cos 2k_{bs}\xi \right) f_\perp^2, \quad (\text{A16})$$

f_\perp is defined by (3.12).

Surface 2R of BS (s-polarization, B_- mode):

$$E_z = \frac{B_-}{\sqrt{2}\sqrt{n}} (e^{ikny_n} - e^{-ikny_n}), \quad (\text{A17a})$$

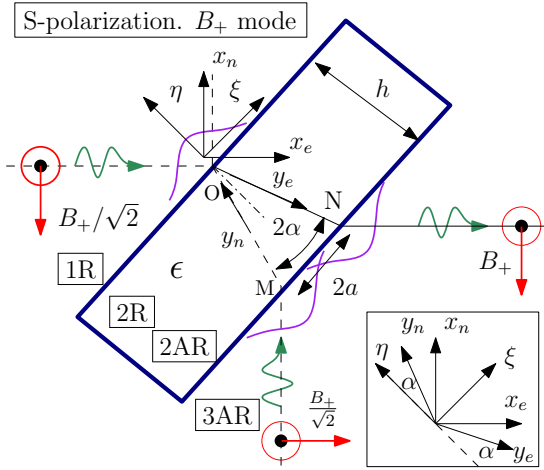


FIG. 5: B_- mode, s-polarization, i.e. the electrical field is normal to the plane of figure, fat dot means that it is directed *out of* plane, cross means *into* the plane. Red arrows relate to complex amplitudes of magnetic fields.

$$E_z|_{\eta=0} = i\frac{\sqrt{2}B_-}{\sqrt{n}} \sin k_{bs}\xi, \quad (\text{A17b})$$

$$H_\eta|_{\eta=0} = -\sqrt{2n}B_- \sin \alpha \cos k_{bs}\xi, \quad (\text{A17c})$$

$$H_\xi|_{\eta=0} = \sqrt{2n}B_- \cos \alpha \cos k_{bs}\xi, \quad (\text{A17d})$$

Maxwell stress tensor on surface 2R:

$$\sigma_{\eta\eta} = \frac{2n|B_-|^2}{4\pi} (-\cos^2 \alpha + \sin^2 \alpha \cos 2k_{bs}\xi). \quad (\text{A18})$$

Here, the component $\sigma_{\eta\eta}$ corresponds to the pressure acting *along* the η -axis, hence $p_\eta = -\sigma_{\eta\eta}$. The spatial distribution of the pressure p_η has to be restored in (A15), by projecting (3.1) on the reflecting surface of the BS:

$$p_\eta^{2rS-} = \frac{2n|B_-|^2}{4\pi} (\cos^2 \alpha - \sin^2 \alpha \cos 2k_{bs}\xi) f_\perp^2. \quad (\text{A19})$$

The total pressure acting on surface R (s-polarization, B_- mode) reads:

$$p_\eta^{rS-} = p_\eta^{1rS-} + p_\eta^{2rS-}, \quad (\text{A20})$$

$$\frac{p_\eta^{rS-}}{\mathcal{E}_-} = \frac{f_\perp^2}{4L} (2n \cos^2 \alpha - 3 - [4\sqrt{2} - 3 + 2n \sin^2 \alpha] \cos 2k_{bs}\xi). \quad (\text{A21})$$

On surface 2AR of the BS (s-polarization, B_- mode): Apparently, in this case the fields will be the same, i.e. equation (A17) can be applied. Hence, equation (A18) for the stress tensor may be applied, but in this case the component $\sigma_{\eta\eta}$ corresponds to pressure acting *along* the η -axis and $p_\eta = \sigma_{\eta\eta}$. The spatial distribution of the pressure p_η on the anti-reflecting surface of the BS is equal to:

$$p_\eta^{2arS-} = \frac{2n|B_-|^2}{4\pi} (-\cos^2 \alpha + \sin^2 \alpha \cos 2k_{bs}\xi_-) f_\perp^2. \quad (\text{A22})$$

Thus, $p_\eta^{2arS-} = -p_\eta^{2rS-}$ (with substitution f_\perp instead of f_-).

Surface 3AR of BS (s-polarization, B_- mode):

$$E_z = \frac{B_-}{\sqrt{2}} (e^{ikx_n} - e^{-ikx_n}), \quad (\text{A23a})$$

$$E_z|_{\eta=0} = i\sqrt{2}B_- \sin k_{bs}\xi_-, \quad (\text{A23b})$$

$$H_\eta|_{\eta=0} = -B_- \cos k_{bs}\xi_-, \quad (\text{A23c})$$

$$H_\xi|_{\eta=0} = B_- \cos k_{bs}\xi_-, \quad (\text{A23d})$$

Maxwell stress tensor on surface 3AR:

$$\sigma_{\eta\eta} = -\frac{|B_-|^2}{4\pi} (1 - \cos 2k_{bs}\xi_-) \quad (\text{A24})$$

$$p_\eta^{3arS-} = \frac{|B_-|^2}{4\pi} (1 - \cos 2k_{bs}\xi_-) f_\perp^2. \quad (\text{A25})$$

Total pressure acting on surface AR (s-polarization, B_- mode):

$$p_\eta^{arS-} = p_\eta^{2arS-} + p_\eta^{3arS-}, \quad (\text{A26})$$

$$\frac{p_\eta^{arS-}}{\mathcal{E}_-} = \frac{f_-^2}{4L} \left(1 + \frac{1}{n} - 2n \right. \\ \left. + \left[\frac{1}{n} - 1 \right] \cos 2k_{bs}\xi_- \right). \quad (\text{A27})$$

3. P-polarization. B_+ mode

On surface 1R of BS (P-polarization, B_+ mode):

$$H_z = \frac{B_+}{\sqrt{2}} (e^{ikx_e} + e^{-ikx_e}), \quad (\text{A28a})$$

$$H_z|_{\eta=0} = \sqrt{2} B_+ \cos k_{bs}\xi, \quad (\text{A28b})$$

$$E_n = \frac{B_+}{\sqrt{2}} (e^{ikx_e} - e^{-ikx_e})_{\eta=0} \\ = i\sqrt{2} B_+ \sin k_{bs}\xi, \quad (\text{A28c})$$

$$E_\xi = E_\eta = \frac{E_n}{\sqrt{2}} = iB_+ \sin k_{bs}\xi. \quad (\text{A28d})$$

Here, B_+ is the amplitude of the electric field in the east arm. Maxwell stress tensor on surface 1R:

$$\sigma_{\eta\eta} = -\frac{|B_+|^2}{4\pi} (1 + \cos \sqrt{2}k\xi). \quad (\text{A29})$$

Component $\sigma_{\eta\eta}$ corresponds to pressure acting *along* the η - axis, hence $p_\eta = \sigma_{\eta\eta}$. The spatial distribution of the pressure p_η should be restored in (A29), by projecting (3.1) on the reflecting surface of the BS by (3.12):

$$p_\eta^{1rP} = -\frac{|B_+|^2}{4\pi} (1 + \cos \sqrt{2}k\xi) f_\perp. \quad (\text{A30})$$

On surface 2R (p-polarization, B_+ mode):

$$H_z = \frac{\sqrt{n}B_+}{\sqrt{2}} (e^{inky_n} + e^{-inky_n}) \quad (\text{A31a})$$

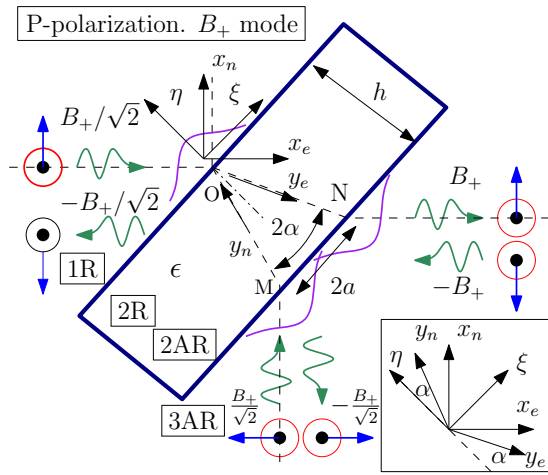


FIG. 6: B_+ mode, p-polarization, i.e. the electric field (blue arrows) is in the plane of figure, the magnetic field is perpendicular to the plane, fat dot means that it is directed *out of* plane, cross means *into* the plane.

$$+ \sqrt{n} B_+ (e^{inky_e} + e^{-inky_e}),$$

$$H_z|_{\eta=0} = \sqrt{2n}(\sqrt{2} + 1)B_+ \cos(k_{bs}\xi), \quad (\text{A31b})$$

$$E_\eta = \frac{B_+ \sin \alpha}{\sqrt{n}\sqrt{2}} (e^{inky_n} - e^{-inky_n}) \quad (\text{A31c})$$

$$+ \frac{B_+}{\sqrt{n}} \sin \alpha (e^{inky_e} - e^{-inky_e}),$$

$$E_\eta|_{\eta=0} = \frac{i\sqrt{2}B_+ \sin \alpha}{\sqrt{n}} (\sqrt{2} + 1) \sin k_{bs}\xi, \quad (\text{A31d})$$

$$E_\xi = -\frac{B_+ \cos \alpha}{\sqrt{n}\sqrt{2}} (e^{inky_n} - e^{-inky_n}) \quad (\text{A31e})$$

$$+ \frac{B_+ \cos \alpha}{\sqrt{n}} (e^{inky_e} - e^{-inky_e}),$$

$$E_\xi|_{\eta=0} = i\frac{\sqrt{2}B_+ \cos \alpha}{\sqrt{n}} (\sqrt{2} - 1) B_+ \sin k_{bs}\xi. \quad (\text{A31f})$$

Maxwell stress tensor on reflecting surface 2R:

$$\sigma_{\eta\eta} = -\frac{n|B_+|^2}{4\pi} \left\{ 6 \cos^2 \alpha \right. \\ \left. + \left(2 \left[\sqrt{2} + 1 \right]^2 - 6 \cos^2 \alpha \right) \cos 2k_{bs}\xi \right\}. \quad (\text{A32})$$

Component $\sigma_{\eta\eta}$ corresponds to pressure acting *along* the η - axis, hence $p_\eta = -\sigma_{\eta\eta}$.

The spatial distribution of pressure p_η should be restored in (A32):

$$p_\eta^{2rP} = \frac{n|B_+|^2}{4\pi} \left\{ 6 \cos^2 \alpha \right. \\ \left. + \left(2 \left[\sqrt{2} + 1 \right]^2 - 6 \cos^2 \alpha \right) \cos 2k_{bs}\xi \right\} f_\perp^2. \quad (\text{A33})$$

Total pressure applied to surface R (p-polarization, B_+ -mode) is equal to *sum* (A30) and (A33):

$$p_\eta^{rP} = p_\eta^{1rP} + p_\eta^{2rP}, \quad (\text{A34})$$

$$\frac{p_\eta^{rP+}}{\mathcal{E}_+} = \frac{f_\perp^2}{4L} \left\{ 6n \cos^2 \alpha - 1 \right. \\ \left. + \left(2n \left[\sqrt{2} + 1 \right]^2 - 6n \cos^2 \alpha - 1 \right) \cos 2k_{bs}\xi \right\}. \quad (\text{A35})$$

On surface 3AR (p-polarization, B_+ mode). Again we have to account that distributions of fields from south arm and east arm are shifted by $\pm a$ (3.16) as shown in Fig. 6:

$$H_z = \frac{B_+}{\sqrt{2}} (e^{ikx_n} + e^{-ikx_n}) f_- \quad (\text{A36a})$$

$$+ B_+ (e^{ikx_e} + e^{-ikx_e}) f_+,$$

$$H_z|_{\eta=-h} = \sqrt{2}B_+ (f_- \cos k_{bs}\xi_-) + \sqrt{2}f_+ \cos k_{bs}\xi_+, \quad (\text{A36b})$$

$$E_\xi = -\frac{B_+}{\sqrt{2}} (e^{ikx_n} - e^{-ikx_n}) \frac{f_-}{\sqrt{2}} \quad (\text{A36c})$$

$$+ B_+ (e^{ikx_e} - e^{-ikx_e}) \frac{f_+}{\sqrt{2}},$$

$$E_\xi|_{\eta=-h} = iB_+ \left(\sqrt{2}f_+ \sin k_{bs}\xi_+ - f_- \sin k_{bs}\xi_- \right), \quad (\text{A36d})$$

$$E_\eta = \frac{B_+}{\sqrt{2}} (e^{ikx_n} - e^{-ikx_n}) \frac{f_-}{\sqrt{2}} + B_+ (e^{ikx_e} - e^{-ikx_e}) \frac{f_+}{\sqrt{2}}, \quad (\text{A36e})$$

$$E_\eta|_{\eta=-h} = iB_+ \left(f_- \sin k_{bs}\xi_- + \sqrt{2}f_+ \sin k_{bs}\xi_+ \right). \quad (\text{A36f})$$

Maxwell stress tensor on anti-reflecting surface 3AR:

$$\begin{aligned} \sigma_{\eta\eta} = & -\frac{|B_+|^2}{4\pi} \left\{ f_-^2 + 2f_+^2 \right. \\ & + 2\sqrt{2}f_-f_+ \cos k_{bs}(\xi_+ + \xi_-) \\ & \left. + \left[f_- \cos 2k_{bs}\xi_- + \sqrt{2}f_+ \cos 2k_{bs}\xi_+ \right]^2 \right\}. \end{aligned} \quad (\text{A37})$$

Pressure along η -axis :

$$p_\eta^{3arP} = -\sigma_{\eta\eta}. \quad (\text{A38})$$

On surface 2AR of the BS (p-polarization, B_+ mode):

$$H_z = \frac{\sqrt{n}B_+}{\sqrt{2}} (e^{inky_n} + e^{-inky_n}) f_- + \sqrt{n}B_+ (e^{inky_e} + e^{-inky_e}) f_+, \quad (\text{A39a})$$

$$H_z|_{\eta=-h} = \sqrt{2n}B_+ \left(f_- \cos k_{bs}\xi_- + \sqrt{2}f_+ \cos k_{bs}\xi_+ \right), \quad (\text{A39b})$$

$$E_\xi = -\frac{B_+}{\sqrt{2n}} (e^{inky_n} - e^{-inky_n}) f_- \cos \alpha + \frac{B_+}{\sqrt{n}} (e^{inky_e} - e^{-inky_e}) f_+ \cos \alpha, \quad (\text{A39c})$$

$$E_\xi|_{\eta=-h} = i\frac{\sqrt{2}B_+}{\sqrt{n}} \cos \alpha \times \left(\sqrt{2}f_+ \sin k_{bs}\xi_+ - f_- \sin k_{bs}\xi_- \right), \quad (\text{A39d})$$

$$E_\eta = \frac{B_+}{\sqrt{2n}} (e^{inky_n} - e^{-inky_n}) f_- \sin \alpha + \frac{B_+}{\sqrt{n}} (e^{inky_e} - e^{-inky_e}) f_+ \sin \alpha, \quad (\text{A39e})$$

$$E_\eta|_{\eta=-h} = \frac{\sqrt{2}B_+}{\sqrt{n}} i \sin \alpha \left(f_- \sin k_{bs}\xi_- + \sqrt{2}f_+ \sin k_{bs}\xi_+ \right). \quad (\text{A39f})$$

Maxwell stress tensor on surface 2AR

$$\begin{aligned} \sigma_{\eta\eta} = & \frac{n|B_+|^2}{2\pi} \left\{ - (f_-^2 + 2f_+^2) \cos^2 \alpha \right. \\ & + \left[- (f_-^2 \cos 2k_{bs}\xi_- + 2f_+^2 \cos 2k_{bs}\xi_+) \sin^2 \alpha \right. \\ & \left. \left. - 2\sqrt{2}f_-f_+ \cos k_{bs}(\xi_- + \xi_+) \right] \right\}. \end{aligned} \quad (\text{A40})$$

Pressure along η -axis:

$$p_\eta^{2arP+} = \sigma_{\eta\eta}. \quad (\text{A41})$$

Total pressure along the η - axis acting on surface AR (p-polarization, B_+ mode) is equal to:

$$p_\eta^{arP+} = p_\eta^{2arP+} + p_\eta^{3arP+} \quad (\text{A42})$$

$$\begin{aligned} \frac{p_\eta^{arP+}}{\mathcal{E}_+} = & \frac{|B_+|^2}{4\pi} \left\{ (f_-^2 + 2f_+^2) \left[1 + \frac{1}{n} - 2n \right] \right. \\ & + \left(4(1-n)\sqrt{2}f_-f_+ \cos k_{bs}(\xi_- + \xi_+) \right. \\ & \left. \left. + (f_-^2 \cos 2k_{bs}\xi_- + 2f_+^2 \cos 2k_{bs}\xi_+) \left(1 - \frac{1}{n} \right) \right) \right\}. \end{aligned} \quad (\text{A43})$$

4. P-polarization. B_- mode

On surface 1R (p-polarization, B_- mode):

$$H_z = \frac{-B_-}{\sqrt{2}} (e^{ikx_e} + e^{-ikx_e}) \quad (\text{A44a})$$

$$+ B_- (e^{ikx_n} + e^{-ikx_n}),$$

$$H_z|_{\eta=0} = \sqrt{2}B_- (\sqrt{2} - 1) \cos k_{bs}\xi, \quad (\text{A44b})$$

$$E_\eta|_{\eta=0} = i(\sqrt{2} - 1) B_- \sin k_{bs}\xi, \quad (\text{A44c})$$

$$E_\xi|_{\eta=0} = -i(1 + \sqrt{2}) B_- \sin k_{bs}\xi, \quad (\text{A44d})$$

Maxwell stress tensor on surface 1R:

$$\sigma_{\eta\eta} = -\frac{|B_-|^2}{4\pi} \left(3 + [3 - 4\sqrt{2}] \cos 2k_{bs}\xi \right). \quad (\text{A45})$$

Component $\sigma_{\eta\eta}$ corresponds to the pressure acting along the η -axis, hence $p_\eta = \sigma_{\eta\eta}$. The spatial distribution of

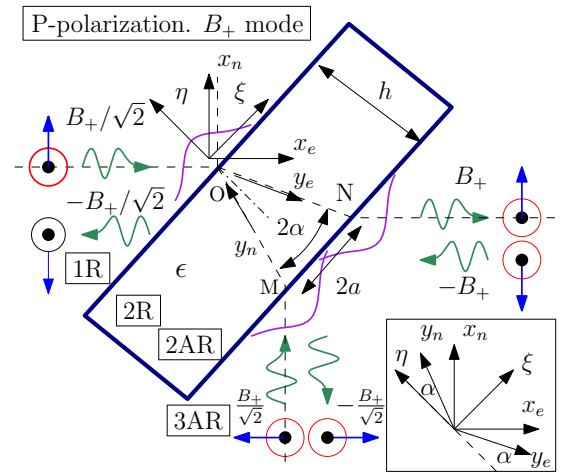


FIG. 7: B_- mode, p-polarization, i.e. the magnetic field is normal to the plane of figure, fat dot means that it is directed into the plane, cross means out of plane. B_- is the amplitude of the electric field in the north arm. Blue arrows indicate the direction of the electric field.

the pressure p_η should be restored in (A45), by projecting (3.1) on surface 1R:

$$p_\eta^{1rP-} = -\frac{|B_-|^2}{4\pi} \times \left(3 + \left[3 - 4\sqrt{2} \right] \cos 2k_{bs}\xi \right) f_\perp^2. \quad (\text{A46})$$

On surface 2R (*s-polarization, B_- mode*):

$$H_z = \frac{\sqrt{n} B_-}{\sqrt{2}} (e^{iky_n} + e^{-iky_n}), \quad (\text{A47a})$$

$$H_z|_{\eta=0} = \sqrt{2n} B_- \cos k_{bs}\xi, \quad (\text{A47b})$$

$$E_\eta|_{\eta=0} = i \frac{\sqrt{2} B_-}{\sqrt{n}} \sin \alpha \sin k_{bs}\xi, \quad (\text{A47c})$$

$$E_\xi|_{\eta=0} = -i \frac{\sqrt{2} B_-}{\sqrt{n}} \cos \alpha \sin k_{bs}\xi, \quad (\text{A47d})$$

Maxwell stress tensor on surface 2R:

$$\sigma_{\eta\eta} = \frac{2n|B_-|^2}{4\pi} (-\cos^2 \alpha - \sin^2 \alpha \cos 2k_{bs}\xi). \quad (\text{A48})$$

Here component $\sigma_{\eta\eta}$ corresponds to pressure acting *along* the η -axis, hence $p_\eta = -\sigma_{\eta\eta}$. The spatial distribution of the pressure p_η should be restored in (A48), by projecting (3.1) on the reflecting surface of the BS:

$$p_\eta^{2rP-} = \frac{2n|B_-|^2}{4\pi} \times (\cos^2 \alpha + \sin^2 \alpha \cos 2k_{bs}\xi) f_\perp^2. \quad (\text{A49})$$

Total pressure acting on surface R (*p-polarization, B_- mode*):

$$p_\eta^{rP-} = p_\eta^{1rP-} + p_\eta^{2rP-}, \quad (\text{A50})$$

$$\frac{p_\eta^{rP-}}{\mathcal{E}_-} = \frac{f_\perp^2}{4L} (2n \cos^2 \alpha - 3 + [4\sqrt{2} - 3 + 2n \sin^2 \alpha] \cos 2k_{bs}\xi). \quad (\text{A51})$$

On surface 2AR (*p-polarization, B_- mode*). In this case equation (A48) for the stress tensor may be applied, but in this case component $\sigma_{\eta\eta}$ corresponds to pressure acting *along* the η -axis and $p_\eta = \sigma_{\eta\eta}$. The spatial distribution of the pressure p_η on the anti-reflecting surface of the BS is equal to:

$$p_\eta^{2arP-} = -\frac{2n|B_-|^2}{4\pi} \times (\cos^2 \alpha + \sin^2 \alpha \cos \sqrt{2}k\xi_-) f_-^2. \quad (\text{A52})$$

Obviously, $p_\eta^{2arP-} = -p_\eta^{2rP-}$.

On surface 3AR (*p-polarization, B_- mode*):

$$H_z = \frac{B_-}{\sqrt{2}} (e^{ikx_n} + e^{-iky_n}), \quad (\text{A53a})$$

$$H_z|_{\eta=0} = \sqrt{2} B_- \cos k_{bs}\xi_-, \quad (\text{A53b})$$

$$E_\eta|_{\eta=0} = iB_- \sin k_{bs}\xi_-, \quad (\text{A53c})$$

$$E_\xi|_{\eta=0} = -iB_- \sin k_{bs}\xi_-. \quad (\text{A53d})$$

Maxwell stress tensor on surface 3AR:

$$\sigma_{\eta\eta} = -\frac{|B_-|^2}{4\pi} (1 + \cos 2k_{bs}\xi_-) \quad (\text{A54})$$

$$p_\eta^{3arP-} = \frac{|B_-|^2}{4\pi} (1 + \cos 2k_{bs}\xi_-) f_-^2. \quad (\text{A55})$$

Total pressure acting on surface AR (*p-polarization, B_- mode*):

$$p_\eta^{arP-} = p_\eta^{2arP-} + p_\eta^{3arP-} \quad (\text{A56})$$

$$\frac{p_\eta^{arP-}}{\mathcal{E}_-} = \frac{f_-^2}{4L} \left(1 - 2n \cos^2 \alpha + [1 - 2n \sin^2 \alpha] \cos 2k_{bs}\xi_- \right). \quad (\text{A57})$$

-
- [1] B. P. Abbott *et al* (LIGO and Virgo Scientific Collaboration), Phys. Rev. Lett. **116**, 061102 (2016).
[2] B. P. Abbott *et al* (LIGO and Virgo Scientific Collaboration), Phys. Rev. Lett. **116**, 241103 (2016).
[3] B. P. Abbott *et al* (LIGO and Virgo Scientific Collaboration), Phys. Rev. Lett. **119**, 161101 (2017).
[4] B. P. Abbott *et al* (LIGO and Virgo Scientific Collaboration), Phys. Rev. Lett. **119**, 141101 (2017).
[5] LVC-Collaboration, arXiv **1304.0670** (2013).
[6] K. Dooley, T. Akutsu, S. Dwyer, and P. Puppò, J. Phys. Conf. Ser. **610**, 012012 (2015).
[7] J. Aasi, B. Abbott, et al., Class. Quantum Grav. **32**, 074001 (2015).
[8] J. Abadie and et. al, Class. Quantum Grav. **32**, 074001 (2015).
[9] F. Acernese et al., Class. Quantum Grav. **32**, 024001 (2015).
[10] H. Grote, Class. Quantum Grav. **27**, 084003 (2010).
[11] V. B. Braginsky, Yu. Levin and S. P. Vyatchanin, Meas. Sci. Technol. **10**, 589606 (1999).
[12] V. B. Braginsky, M. L. Gorodetsky and S. P. Vyatchanin, Phys. Lett. A **264**, 110 (1999).
[13] V. B. Braginsky, M. L. Gorodetsky, S. P. Vyatchanin, Phys. Lett. A **271**, 303307 (2000).
[14] G. Harry, T. Bodiya, and R. Desalvo, eds., Optical Coatings for Precision Measurement (Cambridge University Press, 2012).
[15] R. Nawrodt, S. Rowan, J. Hough, M. Punturo, F. Ricci, and J.-Y. Vinet, Gen. Relativ. Grav. **43**, 593622 (2011).
[16] J. Harms, R. Schnabel, and K. Danzmann, Phys. Rev. D

- 70**, 102001 (2004).
- [17] K. Somiya, LIGO document T0900209 (2009).
- [18] M. Tugolukov, Y. Levin, and S. Vyatchanin, Phys. Lett. A **282**, 2181 (2018).
- [19] H. Callen and T. Welton, Phys. Rev. **83**, 3440 (1951).
- [20] L. Landau and E. Lifshitz, Theoretical Physics: Statistical Physics, Vol. 5 (Butterworth-Heinemann, 1980).
- [21] Y. Levin, Phys. Rev. D **57**, 659663 (1998).
- [22] S. Kroker, J. Dickmann, C. Hurtado, D. Heinert, R. Nawrodt, Y. Levin, and S. Vyatchanin, Phys. Rev. D **96**, 022002 (2017).
- [23] J. Dickmann, C. R. Hurtado, R. Nawrodt, and S. Kroker, Phys. Lett. A **382**, 2275 (2018).
- [24] Y. Demchenko and M.L.Gorodetsky, Moscow University Physics Bulletin **70**, 195002 (2015).
- [25] B. Benthem and Y. Levin, Phys. Rev. D **80**, 062004 (2009).
- [26] C. Law, Phys. Rev. A **51**, 25372541 (1995).
- [27] P. Saulson, Phys. Rev. D **42**, 2437 (1990).
- [28] D. Heinert, K. Craig, H. Grote, S. Hild, H. Luck, R. Nawrodt, D. Simakov, D. Vasilyev, S. Vyatchanin, and H. Wittel, Phys. Rev. D **90**, 042001 (2014).
- [29] www.comsol.com.
- [30] H. Kogelnik and T. Li, Appl. Opt. **5**, 1550 (1966).
- [31] L. Davis, Phys. Rev. A **19**, 11771179 (1979).
- [32] L. Davis and G. Patsakos, Opt. Lett. **61**, 2223 (1981).
- [33] Y. T. Liu and K. S. Thorne, Phys. Rev. D **62**, 122002 (2000).
- [34] R. Adhikari et al., LIGO Document T1400226 (2014).
- [35] D. Coyne, LIGO Document T050057-00-D (2005).
- [36] G. Billingsley, Private Communication (2018).
- [37] H. Lück et al., J. Phys. Conf. Ser. **228**, 012012 (2010).
- [38] H. Grote et al., Class. Quantum Grav. **27**, 084003 (2010).